Results in Physics 8 (2018) 569–577

Contents lists available at ScienceDirect

Results in Physics

journal homepage: www.journals.elsevier.com/results-in-physics

Three dimensional rotating flow of Powell-Eyring nanofluid with non-Fourier's heat flux and non-Fick's mass flux theory

Wubshet Ibrahim

Department of Mathematics, Ambo University, Ambo, Ethiopia

ARTICLE INFO

Article history:
Received 25 October 2017
Received in revised form 25 November 2017
Accepted 11 December 2017
Available online 30 December 2017

Keywords:
Three dimensional flow
Powell-Eyring nanofluid
Rotating flow
Non-Fourier flux theory

ABSTRACT

This article numerically examines three dimensional boundary layer flow of a rotating Powell-Eyring nanofluid. In modeling heat transfer processes, non-Fourier heat flux theory and for mass transfer non-Fick's mass flux theory are employed. This theory is recently re-initiated and it becomes the active research area to resolves some drawback associated with the famous Fourier heat flux and mass flux theory. The mathematical model of the flow problem is a system of non-linear partial differential equations which are obtained using the boundary layer analysis. The non-linear partial differential equations have been transformed into non-linear high order ordinary differential equations using similarity transformation. Employing bvp4c algorithm from matlab software routine, the numerical solution of the transformed ordinary differential equations is obtained. The governing equations are constrained by parameters such as rotation parameter λ, the non-Newtonian parameter N, dimensionless thermal relaxation and concentration relaxation parameters δ_t and δ_c. The impacts of these parameters have been discussed thoroughly and illustrated using graphs and tables. The findings show that thermal relaxation time δ_t reduces the thermal and concentration boundary layer thickness. Further, the results reveal that the rotational parameter λ has the effect of decreasing the velocity boundary layer thickness in both x and y directions. Further examination pinpoints that the skin friction coefficient along x-axis is an increasing and skin friction coefficient along y-axis is a decreasing function of rotation parameter λ. Furthermore, the non-Newtonian fluid parameter N has the characteristic of reducing the amount of local Nusselt numbers $-f''(0)$ and $-g''(0)$ both in x and y -directions.

Introduction

The study of the modified form of Fourier heat flux theory is the recent active research area in fluid heat transfer analysis. The theory is based on the addition of time relaxation term to Fourier heat flux model. The famous Fourier heat conduction theory has a limitation in that it doesn't have a room for time relaxation. Therefore, the recent modified model of the old heat conduction formula believed to be resolving the drawback associated with Fourier heat flux model. Many research activities have been carried out on non-Fourier heat flux model to come up with the possible solution to the drawback. Accordingly, Christove [1] give a new formulation of the Maxwell-Cattaneo model of heat conduction. Besides, Hayat et al. [2] have examined the rotating flow of Jeffery fluid with non-Fourier heat flux model. The finding reveals that the thermal relaxation time reduces the temperature. Further, Hayat et al. [3] studied the characteristics of thermal and concentration diffusion for three dimensional flow of nanofluid using non-Fourier heat flux model. The results of the study signify that thermal and concentration relaxation parameters have a reduction effect on temperature and concentration profiles. Furthermore, Hayat et al. [4] studied a double – diffusion flow of viscoelastic Nanofluids with Cattaneo-Christov model. Moreover, the impact of non-Fourier heat flux on the flow of Maxwell fluid past a stretching sheet with variable thickness was discussed by Hayat et al. [5]. The numerical solution for Sakiadis flow of upper-convected Maxwell fluid using Cattaneo-Christov heat flux model was analyzed by the researchers Mushtaq et al. [6]. Still further, Sui et al. [7] investigated the heat and mass diffusion with Cattaneoe-Christov model in upper-convected Maxwell nanofluid past a stretching sheet with slip velocity boundary condition.

The application of the non-Fourier heat flux model further extended to the more complex non-Newtonian fluid called Carreau fluid and analyzed by Hahim and Khan [8] considering slendering sheet. The numerical investigation of Cattaneo-Christov heat flux mode on the area of a non-Newtonian fluid has got a momentum. In line with this, Khan et al. [9] have examined the effect of

E-mail address: wubshet.ibrahim@ambou.edu.et

https://doi.org/10.1016/j.rinp.2017.12.034
2211-3797/

Nomenclature

C_f	Skin friction coefficient
C_w	Concentration at the surface of the sheet
C_∞	Ambient concentration
D_B	Brownian diffusion coefficient
D_T	Thermophoresis diffusion coefficient
f	Dimensionless stream function
k	Thermal conductivity
k^*	Mean absorption coefficient
Le	Lewis number
M	Magnetic parameter
Nb	Brownian motion parameter
Nt	Thermophoresis parameter
Nu_x	Local Nusselt number
Pr	Prandtl number
Re_x	Local Reynolds number
T	Temperature of the fluid inside the boundary layer
T_w	Temperature at the surface of the sheet
T_∞	Ambient temperature
u, v	Velocity component along x- and y-direction

Greeks

λ_E	The thermal relaxation time
λ_C	The concentration relaxation time
η	Dimensionless similarity variable
ϕ	Dimensionless concentration function
δ_t	thermal relaxation parameter
δ_c	concentration relaxation parameter
μ	Dynamic viscosity of the fluid
υ	Kinematic viscosity of the fluid
$(\rho)_f$	Density of the basefluid
$(\rho c)_f$	Heat capacity of the base fluid
$(\rho c)_p$	Effective heat capacity of a nanoparticle
λ	rotation parameter
ψ	Stream function
θ	Dimensionless tempreture
Γ	The extra stress tensor
Ω	Angular velocity
Λ	Parameter defined by $\frac{(\rho c)_p}{(\rho c)_f}$

Subscripts

∞	Condition at the free stream
w	Condition at the surface

non-Fourier heat flux model on viscoelastic fluid. Furthermore, Abbasi et al. [10] have examined the non-Newtonian Oldroyed-B fluid with variable thermal conductivity employing the Cattaneo-Christove heat flux model. Also, Hayat et al. [11] have applied the Cattaneo-Christov heat flux model on the study of Maxwell fluid with Darcy-Forchheimer flow and variable thermal conductivity. The result reveals that the porosity enhances the velocity and inhibits the temperature. Furthermore, Kahansa and Mustafa [12] have examined MHD three-dimensional flow of upper-convected Maxwell fluid over a bi-directional stretching surface by considering the Cattaneo-Christov heat flux model. Nadeem and Muhammed [13] are also examined the influence of stratification and Cattaneo-Christov heat flux in the flow saturated with porous medium. The findings indicate that an increase in thermal relaxation parameter outcomes in the reduction of the temperature field. Hayat et al. [14] have discussed on doubly stratified chemically reactive flow of non-newtonian fluid called Powell-Eyring liquid subject to time relaxation term on Fourier heat flux theory.It is indicated that thermal and concentration stratification parameters reduces the concentration and concentration graphs. Further, very recently, Liu et al. [15] analyzed heat conduction with fractional Cattaneo-Christov upper-convective derivative flux model. The outcome shows that temperature profiles are monotonically decreases with time fractional parameter with time relaxation parameter. Further examination of the thermal convection with the Cattaneo Christov model has been examined by Straughan [16]. Moreover, the study of Cattaneo-Christove heat flux model was applied to the non-Newtonian fluid called Williamson fluid past a stretching sheet with variable thickness by Salahuddin et al. [17].

The rotating flow of a fluid past a stretching surface has been presented by many scholars. Accordingly, the pioneering study on a rotation flow was discussed by Wang [18]. Later, Kumari and Pop [19] also examined the rotating flow of a non-Newtonian fluid called power-law fluid. The analysis of the study comes up with the result both the x and y-direction skin friction coefficients are reduced by rotation parameter. Further, Shafiq et al. [20] have examined the heat and mass transfer effects of a rotating flow of Maxwell fluid due to stretching surface. Still further, Mustafa [21] examined heat and mass transfer of the rotating flow of Maxwell fluid using Catteneo-Christove heat flux model. The impact of Cattaneo-Christove model on the peristalsis flow was analysed by Tanveer et al. [22]. The stagnation point flow of of Eyring-Powell liquid towards a nonlinear stretched surface with Cattaneo-Christove model was reported by Hayat et al. [23]. Very recently Hayat et al. [24] further examined the effect of the Cattaneo-Christove model on Powell-Eyring fluid with variable thermal conductivity. Again recently, Xiaoqin and Shumei [25] have utilized Cattaneo-Christov heat flux to explore the heat transfer characteristic of Marangoni boundary layer flow in a copper water nanofluid. The comprehensive review of three dimensional flow of different kinds of fluids are given in the references [26–33].

The study of Powell-Eyring nanofluid has not be given wide coverage. Few literatures are available about Powell-Eyring. To list some of them Hayat et al. [34] studied the effect of magnetic field on Powell-Eyring nanofluid past a stretching non-uniform thickness. Javed et al. [35] have discussed the flow of an Eyring-Powell non-Newtonian fluid over a stretching sheet However, the effect of rotation on Powell-Eyring nanofluid with non-Fourier heat flux theory and non-Ficks mass flux theory not yet studied. Therefor, the investigator of the present study aimed to fill the knowledge gape.

Powell-Eyring fluid

In this analysis non-Newtonian fluid called Powell-Eyring fluids is studied. Mathematical modeling of the Powell-Eyring fluid is given by [35]

$$A = -PI + \Gamma \tag{1}$$

where P is the principal stress tensor and Γ is the extra stress tensor and Γ is defined as:

$$\Gamma = \mu A_1 + \frac{1}{\beta\dot{\gamma}} sinh^{-1}\left(\frac{1}{d}\dot{\gamma}\right) A_1 \tag{2}$$

by the same author. Here μ is dynamic viscosity, β and C are the rheological Powell- Eyring fluid model parameters. Using Taylor

series expansion for $sinh^{-1}$ function and taking second order approximation as

$$sinh^{-1}\left(\frac{1}{d}\dot{\gamma}\right) \approx \frac{1}{d}\dot{\gamma} - \frac{1}{6}\left(\frac{1}{d}\dot{\gamma}\right)^3, \quad \left|\frac{1}{d}\dot{\gamma}\right| \ll 1 \tag{3}$$

Hence Eq. (2) takes the form

$$\Gamma = \left(\mu + \frac{1}{\beta d}\right)A_1 - \frac{1}{6\beta d^3}(\dot{\gamma})^3 A_1 \tag{4}$$

where $\dot{\gamma} = \sqrt{\frac{1}{2}trA_1^2}$ and $A_1 = \nabla V + (\nabla V)^T$

Mathematical formulation

The steady viscous and incompressible flow of Powell-Eyring nanofluid past a bi-directional stretching sheet with non-Fourier heat flux theory and non-Fick's mass flux is examined. The characteristics of the nanoparticles are investigated with the condition of passive control of nanoparticles. The coordinate system aligned in xy-plane such that the surface is stretching in both x and y-directions with stretching velocity of $u = ax$, $v = by$, where a and b are constants. Besides, the fluid is considered in the space $z \geqslant 0$. Furthermore, the fluid is allowed to rotates about z-axis with uniform angular velocity Ω. The temperature of the sheet denoted by T_w is constant and assumed to be greater than the ambient temperature T_∞. The concentration of nanoparticles at the surface is give by C_w and the ambient concentration is denoted by C_∞. In this article, the non-Fourier heat flux theory is adopted for heat transfer analysis and non-Fick's mass flux theory for mass transfer.

After boundary layer approximation, the conservation laws of mass, momentum and energy yield the following differential equations as used by Javed et al. [35]

$$\frac{\partial u}{\partial x} + \frac{\partial v}{\partial y} + \frac{\partial w}{\partial z} = 0 \tag{5}$$

$$u\frac{\partial u}{\partial x} + v\frac{\partial u}{\partial y} + w\frac{\partial u}{\partial z} - 2\Omega v = \left(\upsilon + \frac{1}{\rho\beta d}\right)\left(\frac{\partial^2 u}{\partial z^2}\right) - \frac{1}{2\rho\beta d^3}\left(\frac{\partial u}{\partial z}\right)^2\frac{\partial^2 u}{\partial z^2} \tag{6}$$

$$u\frac{\partial v}{\partial x} + v\frac{\partial v}{\partial y} + w\frac{\partial v}{\partial z} + 2\Omega u = \left(\upsilon + \frac{1}{\rho\beta d}\right)\left(\frac{\partial^2 v}{\partial z^2}\right) - \frac{1}{2\rho\beta d^3}\left(\frac{\partial v}{\partial z}\right)^2\frac{\partial^2 v}{\partial z^2} \tag{7}$$

The Fourier's and Fick's law which is called as Catteneo-Christov heat and mass diffusion equations are

$$q + \lambda_E\left(\frac{\partial q}{\partial t} + V\cdot\nabla q - q\cdot\nabla V + (\nabla\cdot V)q\right) = -k\nabla t \tag{8}$$

$$J + \lambda_C\left(\frac{\partial J}{\partial t} + V\cdot\nabla J - J\cdot\nabla V + (\nabla\cdot V)J\right) = -D_B\nabla C \tag{9}$$

where λ_E is the thermal relaxation time and λ_C is the concentration relaxation time. The thermal relaxation time is the delay(lag) required for the beginning of heat flux at some point once a temperature gradient is commenced and similarly, concentration relaxation time is the lag required for the starting of mass flux at some point once a concentration gradient is introduced there.

$$u\frac{\partial T}{\partial x} + v\frac{\partial T}{\partial y} + w\frac{\partial T}{\partial z} + \lambda_E\phi_E = \alpha\left(\frac{\partial^2 T}{\partial z^2}\right) + \tau\left\{D_B\left(\frac{\partial C}{\partial z}\frac{\partial T}{\partial z}\right) + \frac{D_T}{T_\infty}\left[\left(\frac{\partial T}{\partial z}\right)^2\right]\right\} \tag{10}$$

$$u\frac{\partial C}{\partial x} + v\frac{\partial C}{\partial y} + w\frac{\partial C}{\partial z} + \lambda_C\phi_C = D_B\left(\frac{\partial^2 C}{\partial z^2}\right) + \frac{D_T}{T_\infty}\left(\frac{\partial^2 T}{\partial z^2}\right) \tag{11}$$

The boundary conditions are

$$\begin{aligned} &u = u_w(x) = ax, \quad v = v_w(y) = by, \quad w = 0, T = T_w, \\ &D_B\frac{\partial C}{\partial z} + \frac{D_T}{T_\infty}\frac{\partial T}{\partial z} = 0, \quad \text{at} \quad z = 0 \\ &u \to 0, \quad v \to 0, \quad T \to T_\infty, \quad C \to C_\infty \quad \text{as} \quad z \to \infty \end{aligned} \tag{12}$$

where

$$\begin{aligned} \phi_E = {} & u^2\frac{\partial^2 T}{\partial x^2} + v^2\frac{\partial^2 T}{\partial y^2} + w^2\frac{\partial^2 T}{\partial z^2} + 2uv\frac{\partial^2 T}{\partial x\partial y} + 2vw\frac{\partial^2 T}{\partial y\partial z} \\ & + 2uw\frac{\partial^2 T}{\partial x\partial z} + \left(u\frac{\partial u}{\partial x} + v\frac{\partial u}{\partial y} + w\frac{\partial u}{\partial z}\right)\frac{\partial T}{\partial x} \\ & + \left(u\frac{\partial v}{\partial x} + v\frac{\partial v}{\partial y} + w\frac{\partial v}{\partial z}\right)\frac{\partial T}{\partial y} \\ & + \left(u\frac{\partial w}{\partial x} + v\frac{\partial w}{\partial y} + w\frac{\partial w}{\partial z}\right)\frac{\partial T}{\partial z} \end{aligned} \tag{13}$$

$$\begin{aligned} \phi_C = {} & u^2\frac{\partial^2 C}{\partial x^2} + v^2\frac{\partial^2 C}{\partial y^2} + w^2\frac{\partial^2 C}{\partial z^2} + 2uv\frac{\partial^2 C}{\partial x\partial y} + 2vw\frac{\partial^2 C}{\partial y\partial z} \\ & + 2uw\frac{\partial^2 C}{\partial x\partial z} + \left(u\frac{\partial u}{\partial x} + v\frac{\partial u}{\partial y} + w\frac{\partial u}{\partial z}\right)\frac{\partial C}{\partial x} \\ & + \left(u\frac{\partial v}{\partial x} + v\frac{\partial v}{\partial y} + w\frac{\partial v}{\partial z}\right)\frac{\partial C}{\partial y} \\ & + \left(u\frac{\partial w}{\partial x} + v\frac{\partial w}{\partial y} + w\frac{\partial w}{\partial z}\right)\frac{\partial C}{\partial z} \end{aligned} \tag{14}$$

Choosing the following transforms

$$\begin{aligned} &\eta = \sqrt{\frac{a}{\upsilon}}z, \quad u = axf'(\eta), \quad v = ayg'(\eta), \quad w = -\sqrt{a\upsilon}(f(\eta) + g(\eta)) \\ &\theta(\eta) = \frac{T - T_\infty}{T_w - T_\infty}, \quad \phi(\eta) = \frac{C - C_\infty}{C_\infty} \end{aligned} \tag{15}$$

The equation of continuity is synonymously verified and the momentum, energy and concentration equations are reduced to

$$(1+N)f''' - Nk_1(f'')^2 f''' - f'^2 + (f+g)f'' + 2\lambda Lg' = 0 \tag{16}$$

$$(1+N)g''' - Nk_2(g'')^2 g''' - g'^2 + (f+g)g'' - 2\frac{\lambda}{L}f' = 0 \tag{17}$$

$$\theta'' + Pr\left(Nb\theta'\phi' + Nt\theta'^2 + (f+g)\theta' - \delta_t(f+g)(f'+g')\theta' + (f+g)^2\theta''\right) = 0 \tag{18}$$

$$\phi'' + \frac{Nt}{Nb}\theta'' + Sc\left((f+g)\phi' - \delta_c(f+g)(f'+g')\phi' + (f+g)^2\phi''\right) = 0 \tag{19}$$

The boundary conditions are

$$\begin{aligned} &f(0) = 0, \quad f'(0) = 1, \quad g(0) = 0, \quad g'(0) = A, \quad \theta(0) = 1, \\ &Nb\phi'(0) + Nt\theta'(0) = 0, \quad \text{at} \quad \eta = 0, \\ &f'(\infty) \to 0, \quad g'(\infty) \to 0, \quad \theta(\infty) \to 0, \quad \phi(\infty) \to 0, \quad \text{as} \quad \eta \to \infty \end{aligned} \tag{20}$$

where $A = \frac{b}{a}$, $\lambda = \frac{\Omega}{a}$, is the rotation parameter, $L = \frac{\nu}{x}$, $N = \frac{1}{\mu\rho d}$, $M = \frac{\sigma B^2}{\rho a}$, $K = \frac{a^3 x}{2\nu d^2}$, $\delta_t = a\lambda_E$, $\delta_c = a\lambda_C$. where $\lambda = \frac{\Omega}{a}$, $\delta_t = a\lambda_E$ denotes the non dimensional thermal relaxation parameter, Sc stands for Schmidt number and $\delta_c = a\lambda_C$ represents the non dimensional concentration relaxation parameter.

Newton-law is used to derive Skin friction C_f, the Fourier law is employed to derive local Nusselt number Nu_x and the Fick's law is used to define Sherwood numbers Sh_x. Skin friction C_f, local Nusselt Nu_x and Sherwood number Sh_x are represented as follows:

$$C_f = \frac{\tau_w}{\rho u_w^2}, \quad Nu_x = \frac{xq_w}{k(T_w - T_\infty)}, \quad Sh_x = \frac{xh_w}{D(C_w - C_\infty)} \tag{21}$$

The engineering components of this problem are the skin friction coefficients are C_{f_x} and C_{f_y}, local Nusselt number Nu_x and the local Sherwood number Sh_x are defined as:

$$C_{f_x} = \frac{\tau_{w_x}}{\rho u_{w_x}^2}, \quad C_{f_y} = \frac{\tau_{w_y}}{\rho v_{w_y}^2} \quad Nu_x = \frac{xq_w}{k(T_w - T_\infty)}, \quad Sh_x = \frac{xh_w}{D_B(C_w - C_\infty)} \tag{22}$$

where the wall shear stress along x and y axis are τ_{w_x} and τ_{w_y}, wall heat flux q_w and wall mass flux h_m are given by

$$\tau_{w_x} = \mu\left(\frac{\partial u}{\partial z} + \frac{\partial w}{\partial x}\right)_{z=0}, \quad \tau_{w_y} = \mu\left(\frac{\partial v}{\partial z} + \frac{\partial w}{\partial y}\right)_{z=0},$$
$$h_m = -D_B\left(\frac{\partial C}{\partial z}\right)_{z=0}, \quad q_w = -k\left(\frac{\partial T}{\partial z}\right)_{z=0} \tag{23}$$

By using the above equations, we get

$$C_{f_x}\sqrt{Re_x} = (1+N)f''(0) - \frac{1}{3}Nk_1 f'''^3(0),$$
$$C_{f_y}\sqrt{Re_y} = (1+N)g''(0) - \frac{1}{3}Nk_2 g'''^3(0),$$
$$\frac{Nu_x}{\sqrt{Re_x}} = -\theta'(0), \quad \frac{Sh_x}{\sqrt{Re_x}} = -\phi'(0) \tag{24}$$

where Re_x, Re_y, Nu_x, Sh_x are local Reynolds numbers, local Nusselt number and local Sherwood number, respectively.

Numerical solution

This section deals with the numerical solution of the Eqs. (16)–(19) with associated boundary condition equations Eqs. (20). The flow problem is represented by non-linear higher-order a system of ordinary differential equations for which analytical solution is very complex or rarely possible, hence the numerical method is the only possible option for its solution. Hence, a system of differential equation under consideration is a boundary-value problem and it is numerically solved using bvp4c from matlab software.Furthermore, the numerical simulation is carried out using the matlab software to strength the solution obtained.

To apply the method, first transform Eqs. (16)–(19) into a system of first order equations by writing $y_1 = f$, $y_2 = f'$, $y_3 = f''$, $y_4 = g$, $y_5 = g'$, $y_6 = g''$, $y_7 = \theta$, $y_8 = \theta'$, $y_9 = \phi$, $y_{10} = \phi'$. Then the following is obtained:

Then the boundary condition can be written as vector

$$\begin{bmatrix} y_1(0) \\ y_2(0) \\ y_4(0) \\ y_5(0) \\ y_7(0) \\ Nb * y10(0) + Nt * y8(0) \\ y_{inf}(2) \\ y_{inf}(5) \\ y_{inf}(7) \\ y_{inf}(9) \end{bmatrix} = \begin{bmatrix} 0 \\ 0 \\ A \\ 1 \\ 0 \\ 0 \\ 0 \\ 0 \\ 0 \\ 0 \end{bmatrix} \tag{26}$$

The first order system Eqs. (25) can be integrated numerically using bvp4c routine in matlab by assigning the appropriate value for the missing values.

This method has an advantage that it can easily programmed in the matlab with the utilization of the matlab routine.

Analysis of the results and discussions

This section is aimed to analyze the impact of governing parameters on the flow field, temperature and concentration profiles. At the outset of the section, the comparison of $-f''(0)$ with the existing result from review of literature when the fluid is non-rotating frame (see Table 1) is compared. The results are convincing for all parameters taken into consideration. Table 2 illustrates the impact of different governing parameters on skin friction coefficient along x and y-axis directions. One can easily notice that the skin friction coefficient along x-axis is a decreasing function of the parameters such as α, N and λ and increasing function of the parameters k_1 and k_2. The skin friction coefficient along y-axis shows the characteristics of an increment along as the parameters such as α, k_2 and λ and the opposite behaviour is observed for the parameters such as k_1 and N. Table 3 shows that the variation of heat transfer rate as the values of δ_t and λ varies. Accordingly, the values of $-\theta(0)$ increases as the values of δ_t increases and decreases as the value of rotation parameter λ increases.

The next section presents the analysis based on the graphical results. Fig. 1 portraits the influence of non-Newtonian parameter N and rotation parameter λ on non-dimensional velocity along x-axis direction. The non-Newtonian parameter N act as inducing agent in an increment of velocity boundary layer thickness whereas the rotation parameter acts in opposite manner.

$$\begin{bmatrix} y_1' \\ y_2' \\ y_3' \\ y_4' \\ y_5' \\ y_6' \\ y_7' \\ y_8' \\ y_9' \\ y_{10}' \end{bmatrix} = \begin{bmatrix} y(2) \\ y(3) \\ (y(2)^2 - (y(1)+y(4)) * y(3) - 2 * L * La * y(5))/(1 + N - N * k1 * y(3)^2) \\ y(5) \\ y(6) \\ (y(5)^2 - (y(1)+y(4)) * y(6) + 2 * (La/L) * y(2))/(1 + N - N * k2 * y(6)^2) \\ y(8) \\ -Pr * (Nb * y(8) * y(10) + Nt * y(8)^2 + (y(1)+y(4)) * y(8) - Dt * (y(1)+y(4)) * (y(2)+y(5)) \\ * y(8))/(1 - Dt * Pr * (y(1)+y(4))^2) \\ y(10) \\ ((Nt/Nb) * (Pr * (Nb * y(8) * y(10) + Nt * y(8)^2 + (y(1)+y(4)) * y(8) - Dt * (y(1)+y(4)) * (y(2)+y(5)) \\ * y(8))/(1 - Dt * Pr * (y(1)+y(4))^2)) - Sc * ((y(1)+y(4)) * y(10) - Dc \\ * (y(1)+y(4)) * (y(2)+y(5)) * y(10)))/(1 - Sc * Dc * (y(1)+y(4))^2) \end{bmatrix} \tag{25}$$

Table 1
The comparison of the present computed values of $-f''(0)$ for different values of k_1 and N when $\alpha = \lambda = 0$ with the previous study result by [35].

k_1/N	0.0	0.2	0.4	0.6	0.8	1
(Present result)						
0.0	1	0.9129	0.8452	0.7906	0.7454	0.7071
0.1	1	0.9159	0.8493	0.7951	0.7498	0.7115
0.2	1	0.9190	0.8536	0.7997	0.7545	0.7159
0.3	1	0.9222	0.8581	0.8046	0.7594	0.7206
0.4	1	0.9254	0.8627	0.8097	0.7644	0.7255
0.5	1	0.9288	0.8675	0.8150	0.7698	0.7307
0.6	1	0.9322	0.8725	0.8206	0.7754	0.7361
0.7	1	0.9358	0.8778	0.8265	0.7814	0.7419
0.8	1	0.9394	0.8833	0.8327	0.7878	0.7480
0.9	1	0.9431	0.8891	0.8394	0.7946	0.7546
1.0	1	0.9470	0.8952	0.8464	0.8018	0.7616
The Ref. [35] result						
0.0	1	0.9129	0.8452	0.7906	0.7454	0.7071
0.1	1	0.9159	0.8493	0.7951	0.7498	0.7115
0.2	1	0.9190	0.8536	0.7997	0.7545	0.7159
0.3	1	0.9222	0.8581	0.8046	0.7594	0.7206
0.4	1	0.9254	0.8627	0.8097	0.7644	0.7255
0.5	1	0.9288	0.8675	0.8150	0.7698	0.7307
0.6	1	0.9322	0.8725	0.8206	0.7754	0.7361
0.7	1	0.9358	0.8778	0.8265	0.7814	0.7419
0.8	1	0.9394	0.8833	0.8327	0.7878	0.7480
0.9	1	0.9431	0.8891	0.8394	0.7946	0.7546
1.0	1	0.9470	0.8952	0.8464	0.8018	0.7616

Table 2
The computed values of $-f''(0)$ and $-g''(0)$ for different values of $k_1, k_2, N, \alpha, \lambda$.

α	k_1	k_2	N	λ	$-f''(0)$	$-g''(0)$
0	0.5	0.5	0.5	0.5	0.9847	0.5211
0.25					0.8841	0.6543
0.5					0.8094	0.8653
0.75					0.7503	1.1524
0.5	0.1				0.7945	0.8686
	0.2				0.7980	0.8678
	0.3				0.8017	0.8670
	0.4				0.8055	0.8662
	0.5				0.8094	0.8653
	0.5	0.1			0.8077	0.8407
		0.2			0.8081	0.8464
		0.3			0.8085	0.8524
		0.4			0.8090	0.8587
		0.5			0.8094	0.8653
		0.5	0.1		0.9298	0.9903
			0.2		0.8959	0.9556
			0.3		0.8647	0.9232
			0.4		0.8359	0.8932
			0.5		0.8094	0.8653
			0.5	0.2	0.8457	0.5751
				0.3	0.8255	0.6755
				0.4	0.8144	0.7726
				0.5	0.8094	0.8653

Table 3
The computed values of $-\theta'(0)$ for different values of δ_t and rotation parameter λ.

δ_t	0.0	0.1	0.2	0.3	0.4	0.5
$-\theta'(0)$	0.6674	0.6827	0.6990	0.7165	0.7353	0.7555
λ	0.0	0.1	0.2	0.3	0.4	0.5
$-\theta'(0)$	–	–	0.8279	0.8060	0.7814	0.7555

Physically the rotation parameter reduces its linear velocity because, while the fluid is rotating and flowing, its velocity is reduced rotational friction force induced by flow. Fig. 2 also shows the impact of rotation on both x and y-directions velocity. In both directions, the velocities are reduced by rotation parameter. The graph also shows that the reduction in y-direction is more than in x-direction. This indicates that retarding force along y-direction is more than in x-direction.

Fig. 3 sketches the variation of x-direction velocity for different stretching ratio α when the fluid is rotating and not rotating. When the stretching ratio increases for rotating flow, it enhance velocity and inhibit the velocity otherwise.

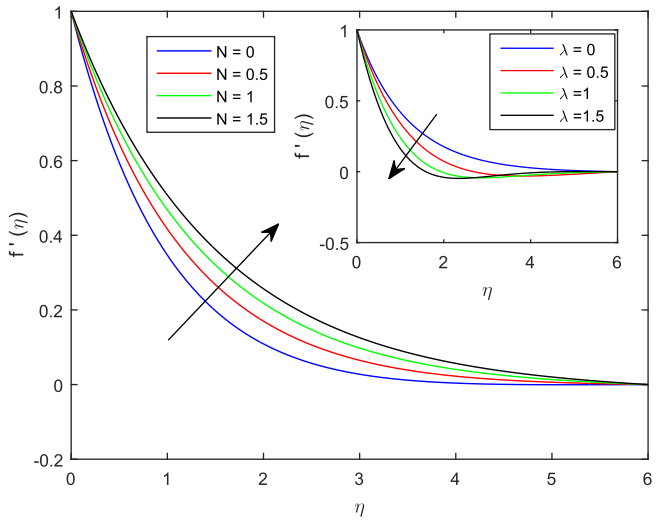

Fig. 1. The velocity profile graph along x direction for different values of rotation stretching ratio λ and Non-newtonian parameter N.

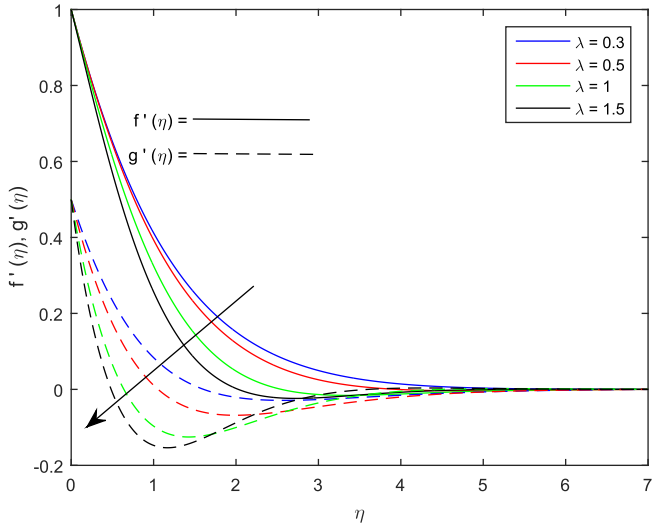

Fig. 2. The velocity profile graph along x and y direction for different values of rotation stretching ratio λ and Non-newtonian parameter N.

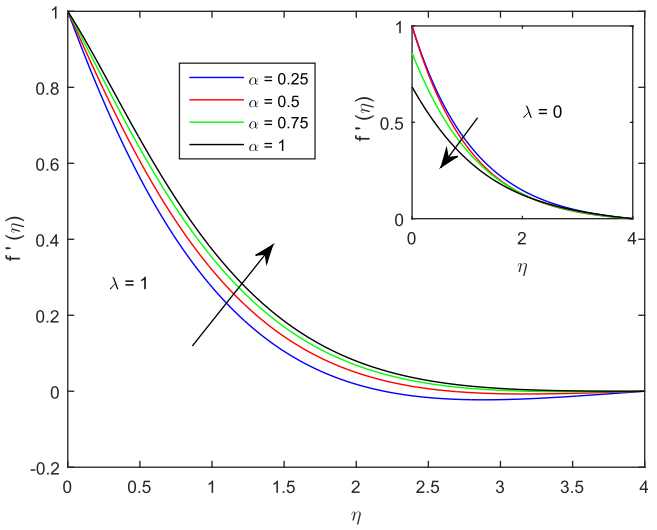

Fig. 3. The velocity profile graph along x axis for different values of stretching ratio α when is rotating and not rotating.

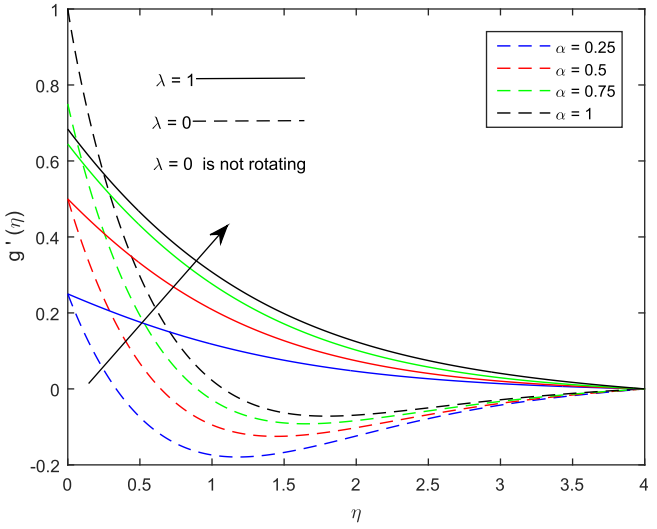

Fig. 4. The velocity profile graph along y-axis for different values of stretching ratio α when is rotating and not rotating.

Fig. 4 illustrates the profile graph of non-dimensional velocity along y-axis. The rotation parameter α favours the y-directional velocity. Fig. 5 shows the sensitiveness of velocity profiles along the ratio of $L = \frac{y}{x}$. As the values of L increases both x and y -direction dimensionless velocities f' and g' are increasing functions. Fig. 6 represents the velocity profile along y-direction as the fluid is rotating not rotating as non-Newtonian parameter N increases. Whether the fluid is rotating or not, as non-Newtonian parameter N increases, the velocity in y-direction increases.But the degree of an increment in y-direction velocity is more when the fluid is not rotating.

Fig. 7 is the pictorial representation of the effects of rotation parameter λ for the fluid under consideration. As it can bee seen from the graph, as the rotation parameter λ increases,the temperature rises. An increment in temperature is more when the fluid is Newtonian. This shows that the non-Newtonian parameter N can facilitates the transfer of heat in the boundary layer.

Fig. 8 indicates the variation of temperature graph as the time relaxation parameter δ_t (Cattaneo-Christov heat flux model) and Prandtl number parameter increases. The graph shows as the values of δ_t increases, the heat transfer increases, as a result the thermal boundary layer thickness decreases. As indicated in different literatures, as Prandtl number Pr increases, the heat transfer is increased as a result, thermal boundary layer is thinner.

The variation of temperature field for different values of thermophoresis parameter Nt and non-Newtonian parameter N is sketched in Fig. 9. From the figure, we can see that as the values of Nt increase the thermal boundary layer thickness increases and the opposite effect is observed for non-newtonian parameter N.

Figs. 10–13 explain the impact of different parameters such as rotation parameter λ, time relaxation parameter δ_t, concentration relaxation parameter δ_c, non-newtonian parameter N, Schmidt number parameter SC Brownian motion parameter Nb on the concentration graphs. Fig. 10 shows the influence of rotation on Newtonian and non-Newtonian fluids. The comparison revels that the non-Newtonian fluid resist rotation than the Newtonian fluid. The graph further demonstrate that, the concentration boundary layer thickness is favored by rotation parameter λ.

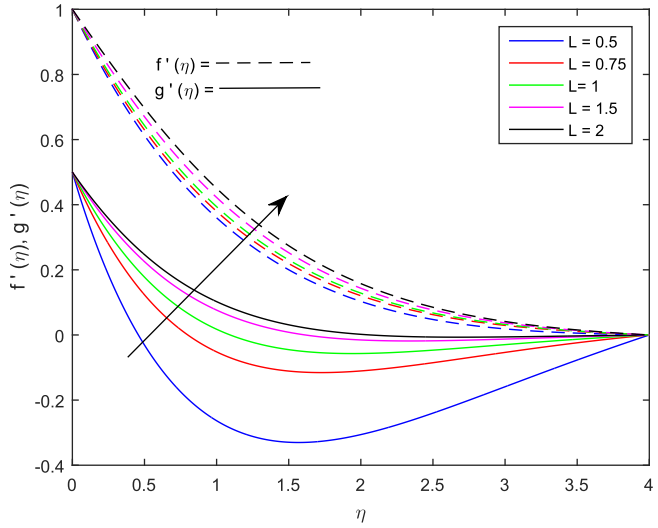

Fig. 5. The velocity profile along x and y direction for different values of L when it is rotation.

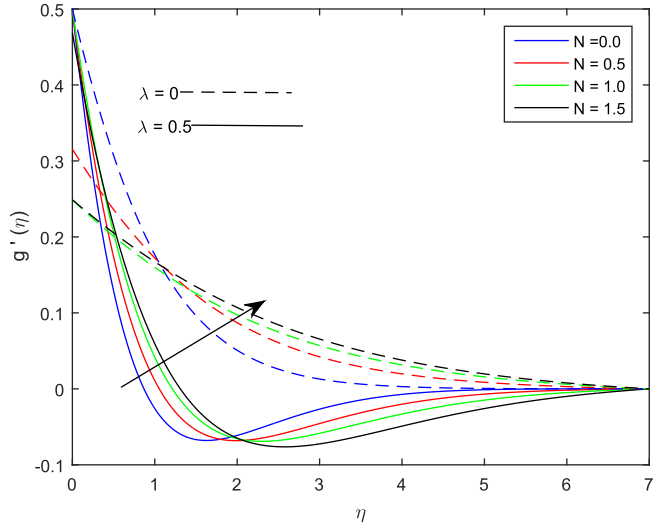

Fig. 6. The velocity profile along y direction for different values of N when it is rotation and not rotating.

Fig. 11 is a double graph which explaining the variation of concentration graph with time relaxation for heat diffusion δ_t and time relaxation for mass diffusion δ_c. The concentration boundary layer thickness decreases as both parameters δ_t and δ_c increase in values for Powel-Erying fluid.

Fig. 12 shows the concentration graph for different values parameters Sc and Nb. As the values of both parameters equally increase, the concentration boundary layer thickness is more influenced by Brownian motion then the Schmidt number Sc.

Fig. 13 illustrate the influences of non-Newtonian parameter N on the concentration graph. As the degree of non-Newtonian's increases, the boundary layer thickness more reduces.

Figs. 14 and 15 sketch the graph of skin friction coefficient along x-axis and y-axis respectively for different values of non-newtonian parameter N along k1 and k2. The graph of skin friction coefficient along the two axis is an increasing function of non-newtonian parameter N and a decreasing function of the parameters k1 and k2.

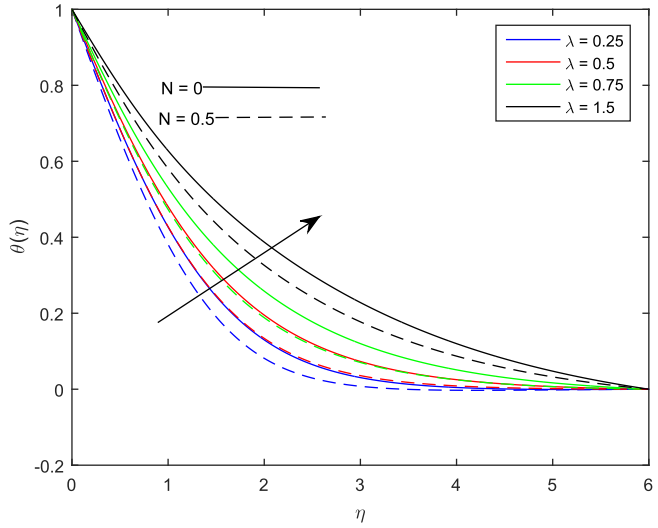

Fig. 7. The temperature graph for different values of rotation parameter λ.

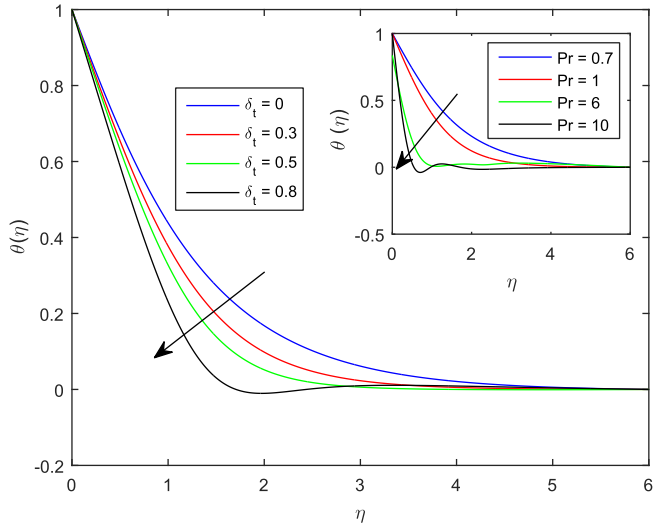

Fig. 8. The temperature graph for different values of Pr and δ_t.

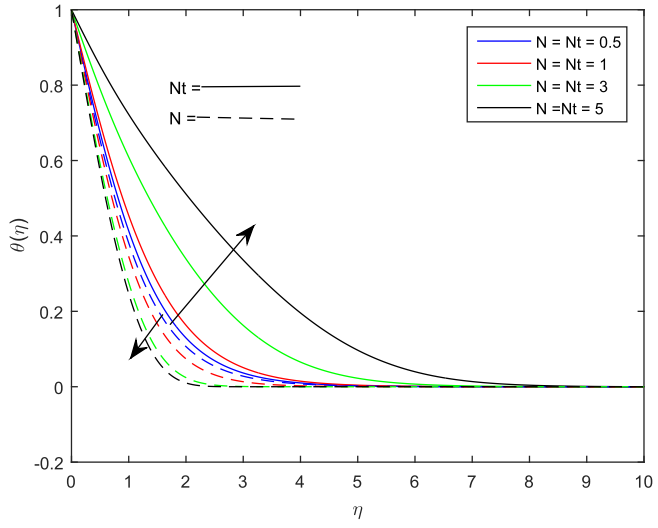

Fig. 9. The temperature graph for different values of thermophoresis parameter Nt and N.

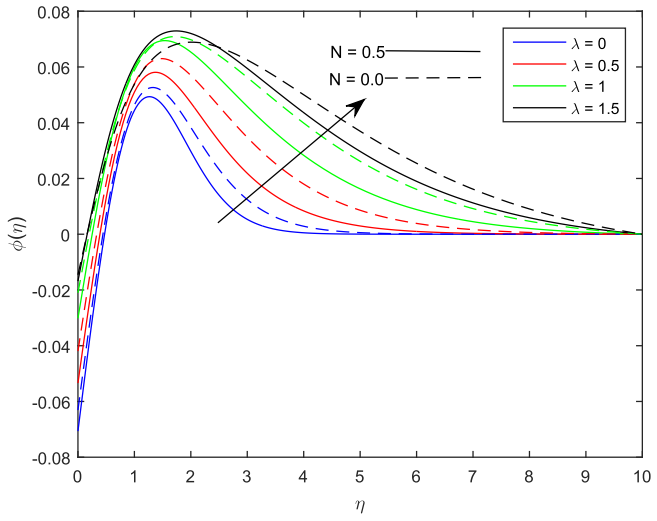

Fig. 10. The concentration graph for different values of rotation parameter λ when $N = 0$ and $N = 0.5$.

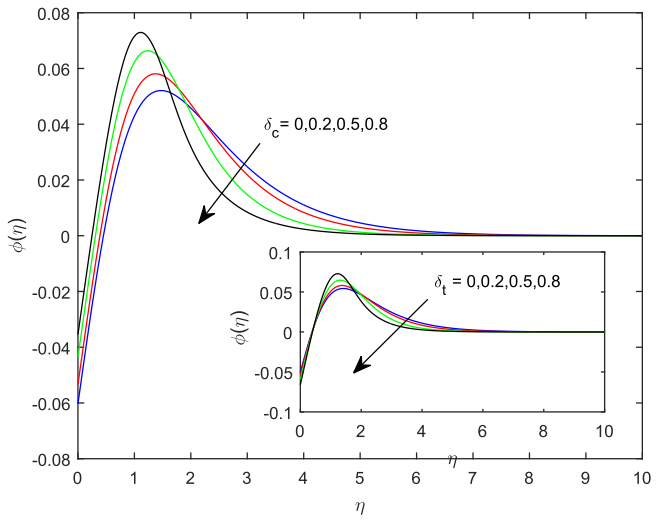

Fig. 11. The concentration graph for different values of parameters δ_c and δ_t when $N = 0.5$.

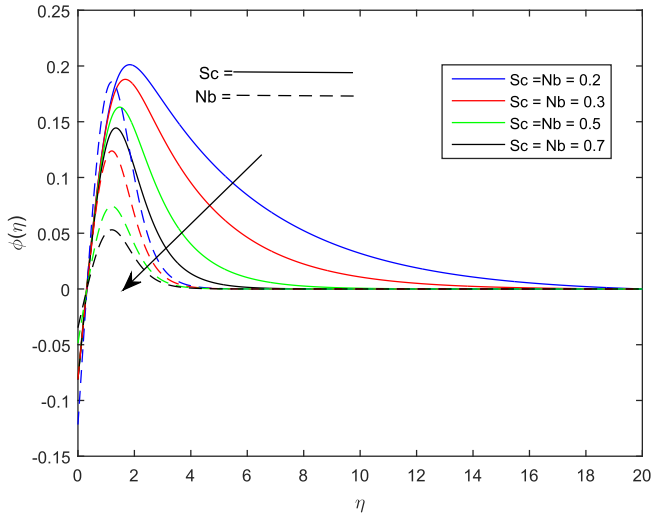

Fig. 12. The concentration graph for different values of Sc and Nb when $N = 0.5$.

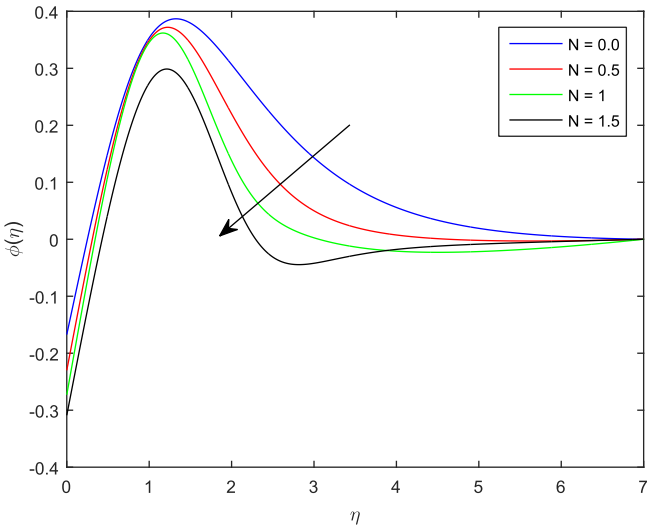

Fig. 13. The concentration graph for different values of N when $Nb = Nt = 0.3$.

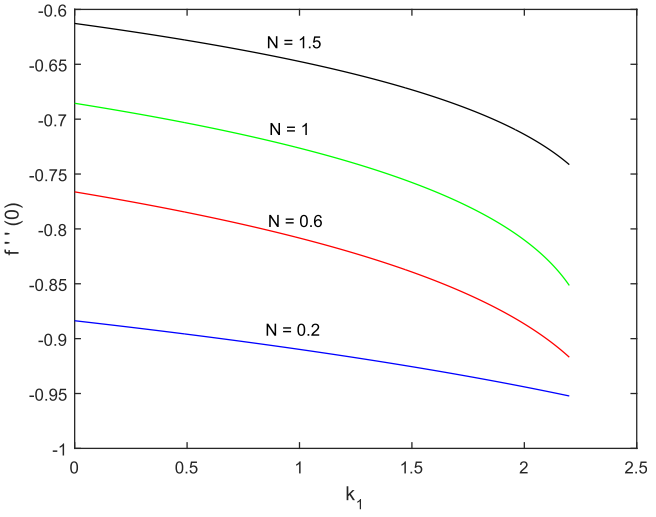

Fig. 14. The graph of skin friction coefficient along x-axis $f''(0)$ for different values of N when $Nb = Nt = 0.3$.

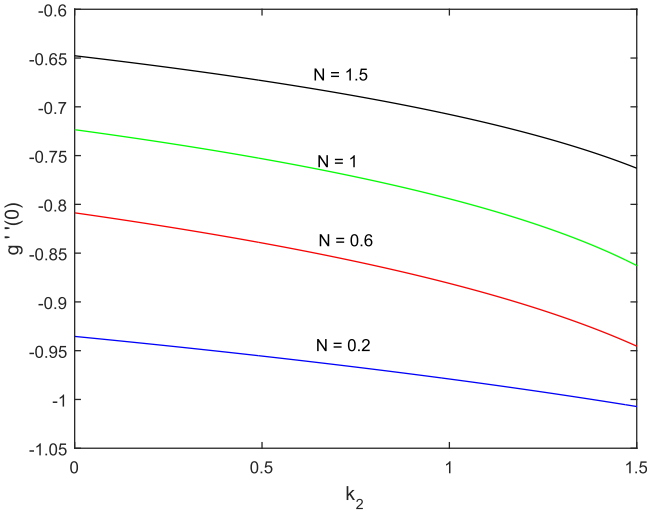

Fig. 15. The graph of skin friction coefficients along y-axis $g''(0)$ for different values of N when $Nb = Nt = 0.3$.

Concluding observations

The revolving Powell-Eyring nanofluid past a bi-directional stretching surface is numerically studied. The Cattaneo-Christov heat flux model is employed for heat transfer analysis. Some of the key observations in this study are:

1. The rotation parameter λ has a characteristic of reducing the hydrodynamics boundary layer thickness.
2. The rotation parameter λ reduces the heat transfer on the boundary layer.
3. The influences of rotation parameter λ is more in Newtonian fluid then non-Newtonian case.
4. Thermal relaxation parameter δ_t reduces the thermal boundary layer thickness.
5. δ_t and δ_c have a similar effect on the concentration graph.
6. The skin friction coefficient $-f''(0)$ more developed as non-Newtonian parameter increases.
7. Non-Newtonian parameter N reduces the skin friction coefficient along both x and y-axis.
8. Time relaxation parameter δ_t initiates the local Nusselt number.

References

[1] Christov C. On frame indifferent formulation of the Maxwell–Cattaneo model of finite-speed heat conduction. Mech Res Commun 2009;36:481–6.
[2] Hayat T, Qayyum S, Imtiaz M, Alsaedi A. Three-dimensional rotating flow of jeffrey fluid for cattaneo-christov heat flux model. AIP Adv 2016;6. 025012.
[3] Hayat T, Muhammad T, Alsaedi A, Ahmad B. Three-dimensional flow of nanofluid with Cattaneo–Christov double diffusion. Results Phys 2016;6:897–903.
[4] Hayat T, Aziz A, Muhammad T, Alsaedi A. Model and comparative study for flow of viscoelastic nanofluids with Cattaneo-Christov double diffusion. PLoS One 2017;12. e0168824.
[5] Hayat T, Farooq M, Alsaedi A, Al-Solamy F. Impact of cattaneo-christov heat flux in the flow over a stretching sheet with variable thickness. AIP Adv 2015;5. 087159.
[6] Mushtaq A, Abbasbandy S, Mustafa M, Hayat T, Alsaedi A. Numerical solution for sakiadis flow of upper-convected maxwell fluid using Cattaneo-Christov heat flux model. AIP Adv 2016;6. 015208.
[7] Sui J, Zheng L, Zhang X. Boundary layer heat and mass transfer with Cattaneo–Christov double-diffusion in upper-convected maxwell nanofluid past a stretching sheet with slip velocity. Int J Therm Sci 2016;104:461–8.
[8] Khan M et al. On Cattaneo-Christov heat flux model for carreau fluid flow over a slendering sheet. Results Phys 2016.
[9] Khan JA, Mustafa M, Hayat T, Alsaedi A. Numerical study of cattaneo-christov heat flux model for viscoelastic flow due to an exponentially stretching surface. PLoS One 2015;10. e0137363.
[10] Abbasi FM, Shehzad SA, Hayat T, Alsaedi A, Hegazy A. Influence of Cattaneo-Christov heat flux in flow of an oldroyd-b fluid with variable thermal conductivity. Int J Numer Methods Heat Fluid Flow 2016;26: 2271–82.
[11] Hayat T, Muhammad T, Al-Mezal S, Liao S. Darcy-forchheimer flow with variable thermal conductivity and Cattaneo-Christov heat flux. Int J Numer Methods Heat Fluid Flow 2016;26:2355–69.
[12] Rubab K, Mustafa M. Cattaneo-Christov heat flux model for mhd three-dimensional flow of maxwell fluid over a stretching sheet. PLoS One 2016;11. e0153481.
[13] Nadeem S, Muhammad N. Impact of stratification and cattaneo-christov heat flux in the flow saturated with porous medium. J Mol Liq 2016;224:423–30.
[14] Hayat T, Zubair M, Waqas M, Alsaedi A, Ayub M. On doubly stratified chemically reactive flow of Powell–Eyring liquid subject to non-fourier heat flux theory. Results Phys 2016.
[15] Liu L, Zheng L, Liu F, Zhang X. Heat conduction with fractional Cattaneo–Christov upper-convective derivative flux model. Int J Therm Sci 2017;112:421–6.
[16] Straughan B. Thermal convection with the Cattaneo–Christov model. Int J Heat Mass Transfer 2010;53:95–8.
[17] Salahuddin T, Malik MY, Hussain A, Bilal S, Awais M. Mhd flow of Cattanneo–Christov heat flux model for williamson fluid over a stretching sheet with variable thickness: using numerical approach. J Magn Magn Mater 2016;401:991–7.
[18] Wang C. Stretching a surface in a rotating fluid. Zeitschrift für Angewandte Mathematik und Physik (ZAMP) 1988;39:177–85.
[19] Kumari M, Grosan T, Pop I. Rotating flow of power-law fluids over a stretching surface. Technische Mechanik 2006;26:11–9.
[20] Shafique Z, Mustafa M, Mushtaq A. Boundary layer flow of maxwell fluid in rotating frame with binary chemical reaction and activation energy. Results Phys 2016;6:627–33.
[21] Mustafa M. Cattaneo-Christov heat flux model for rotating flow and heat transfer of upper-convected maxwell fluid. AIP Adv 2015;5. 047109.
[22] Tanveer A, Hina S, Hayat T, Mustafa M, Ahmad B. Effects of the Cattaneo–Christov heat flux model on peristalsis. Eng Appl Comput Fluid Mech 2016;10:373–83.
[23] Hayat T, Zubair M, Ayub M, Waqas M, Alsaedi A. Stagnation point flow towards nonlinear stretching surface with Cattaneo-Christov heat flux. Eur Phys J Plus 2016;131:355.
[24] Hayat T, Khan MI, Waqas M, Alsaedi A. On Cattaneo–Christov heat flux in the flow of variable thermal conductivity Eyring–Powell fluid. Results Phys 2017.
[25] Xu X, Chen S. Cattaneo–Christov heat flux model for heat transfer of marangoni boundary layer flow in a copper–water nanofluid. Heat Transfer Asian Res 2017.
[26] Hayat T, Aziz A, Muhammad T, Alsaedi A. On magnetohydrodynamic three-dimensional flow of nanofluid over a convectively heated nonlinear stretching surface. Int J Heat Mass Transfer 2016;100:566–72.
[27] Muhammad T, Alsaedi A, Hayat T, Shehzad SA. A revised model for darcy-forchheimer three-dimensional flow of nanofluid subject to convective boundary condition. Results Phys 2017;7:2791–7.
[28] Hayat T, Muhammad T, Shehzad S, Alsaedi A. Three dimensional rotating flow of maxwell nanofluid. J Mol Liq 2017;229:495–500.
[29] Hayat T, Ahmed S, Muhammad T, Alsaedi A, Ayub M. Computational modeling for homogeneous-heterogeneous reactions in three-dimensional flow of carbon nanotubes. Results Phys 2017;7:2651–7.
[30] Hayat T, Aziz A, Muhammad T, Alsaedi A. Three-dimensional flow of nanofluid with heat and mass flux boundary conditions. Chin J Phys 2017.
[31] Hayat T, Muhammad T, Alsaedi A, Alhuthali M. Magnetohydrodynamic three-dimensional flow of viscoelastic nanofluid in the presence of nonlinear thermal radiation. J Magn Magn Mater 2015;385:222–9.
[32] Ibrahim W. Magnetohydrodynamics (mhd) flow of a tangent hyperbolic fluid with nanoparticles past a stretching sheet with second order slip and convective boundary condition. Results Phys 2017;7:3723–31.
[33] Hayat T, Muhammad T, Mustafa M, Alsaedi A. An optimal study for three-dimensional flow of maxwell nanofluid subject to rotating frame. J Mol Liq 2017;229:541–7.
[34] Hayat T, Ullah I, Alsaedi A, Farooq M. Mhd flow of powell-eyring nanofluid over a non-linear stretching sheet with variable thickness. Results Phys 2017;7:189–96.
[35] Javed T, Ali N, Abbas Z, Sajid M. Flow of an Eyring-Powell non-newtonian fluid over a stretching sheet. Chem Eng Commun 2013;200:327–36.